

RESEARCH ON FIELD EMISSION AND DARK CURRENT IN ILC CAVITIES

Y. Li^{1,2}, K. Liu¹, R. Geng², A. Palczewski²

¹ Institute of Heavy Ion Physics, Peking University, Beijing, 100871, China

² Jefferson Laboratory, Newport News, VA 23606, U.S.A.

Abstract

Field emission and dark current are issues of concern for SRF cavity performance and SRF linac operation. Complete understanding and reliable control of the issue are still needed, in particular in full-scale multi-cell practical cavities. Our work aims at developing a generic procedure for finding an active field emitter in a multi-cell cavity and benchmarking the procedure through cavity vertical testing. Our ultimate goal is to provide feedback to cavity preparation and cavity string assembly in order to reduce or eliminate field emission in multi-cell cavities assembled into cryomodules.

Systematic analysis of behaviors of field emitted electrons is obtained using the ACE3P code developed by SLAC. Experimental benchmark of the procedure was carried out in cryogenic testing of a 9-cell cavity in a vertical dewar at JLab's VTA facility. The energy spectrum of Bremsstrahlung X-rays is measured using a NaI(Tl) crystal placed above the top plate of the Dewar. The end-point energy in the X-ray energy spectrum is taken as the highest kinetic electron energy, allowing the prediction of the longitudinal position of the active field emitter. Angular location of the field emitter is determined by placing an array of silicon diodes around irises of the cavity which is immersed in liquid helium. Following the cryogenic RF testing, high-resolution optical inspection was conducted at the predicted field emitter location.

INTRODUCTION

The ILC baseline design cavity is a standing wave structure of about 1m in length operating at TM010 π mode [1]. A sketch of the cavity is shown in Fig.1. The ILC project requires high accelerating gradient cavity for TeV electron collider. With high field gradient, field emission and dark current become potential serious limiting factors to SRF cavities performance. Additional heat load to cavity and hence to the cryogenic system are caused by field emission electrons. Some kind of field emission electrons can pass through the cavity and gain high energy over long distance. These kinds of electrons are dangerous and they might cause activation of the cavity [2] or accelerator components [3]. In most cases, the cause and location of the emitter are not clear during cavity RF test. Our work aims at developing a generic procedure for finding an active field emitter in a multi-cell cavity and benchmarking the procedure through cavity vertical testing.

FIELD EMISSION SIMULATION TOOL

The electromagnetic codes ACE 3P developed at SLAC are based on high-order Parallel Finite Element method for geometry fidelity and simulation accuracy [4]. ACE 3P includes Omega 3P eigmodesolver and Track 3P a particle tracking code. In our simulation, Omega 3P was used to get the field distribution in the cavity. Using fields by Omega3P, simulation of field emission are carried out by Track3P. This code has been benchmarked by SLAC dark current simulation and their experiment [5].

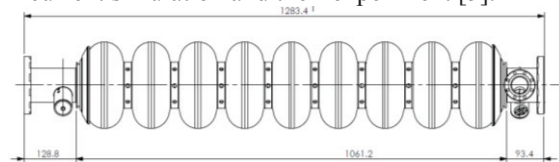


Fig. 1: TESLA 9cell cavity.

In particle track simulation, electrons are launched from specific surfaces at different phases during one radiofrequency (RF) period. The current from a field emitter is generated according to Fowler-Nordheim equation [6] (see equation 1).

$$I(E) = \frac{A_{FN} A_e (\beta_{FN} E)^2}{\varphi} \exp\left(-\frac{B_{FN} \varphi^2}{\beta_{FN} E}\right) \quad (1)$$

Where $A_{FN} = 1.54 \cdot 10^6$, $B_{FN} = 6.83 \cdot 10^4$, A_e is emitter area, φ is the work function of niobium, β_{FN} is the field enhancement factor. In simulation, $\varphi = 4.2$, $\beta_{FN} = 150$, a value that has typically been found in other measurements [7,8,9]. The initial launched electrons follow the electromagnetic fields in the structure and eventually hit the boundary. The secondary electrons are still tracked. But in our simulation, we did not consider the secondary electron yield and SEY curve was set to 0.

SIMULATION RESULT OF FIELD EMISSION ELECTRONS DISTRIBUTION

The π mode surface electric field of a TESLA 9 cell cavity is shown in Fig. 2. The surface electric field around iris is much higher than other places. In our simulation, the emitted electrons are launched from the area near the iris (see Fig. 3).

As an example, iris-5 was selected to launch emission electrons at the accelerating gradient of 15MV/m. To simplify the discussion, a local coordinate was used as a function of distance (S) from the center of each iris along the cavity wall (see Fig. 4). So, an emitter position is specified by the iris number and local coordinate (S). In the following discussion, iris was short for IR. So,

IR_5_LF mean left side (LF) of iris 5 and IR_5_RT means right side (RT) of iris 5.

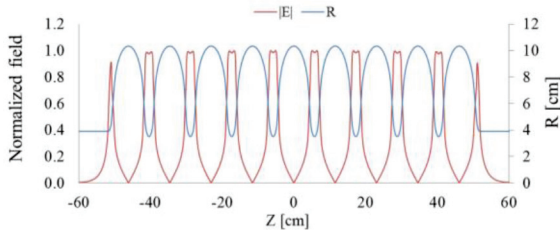


Fig. 2: π mode surface electric field (blue line) and cavity shape (brown line) of TESLA 9cell cavity.

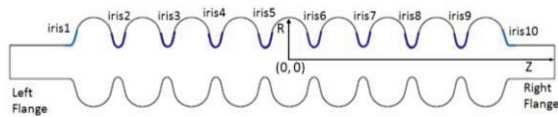


Fig. 3: Field emission simulation area at different iris (Blue area).

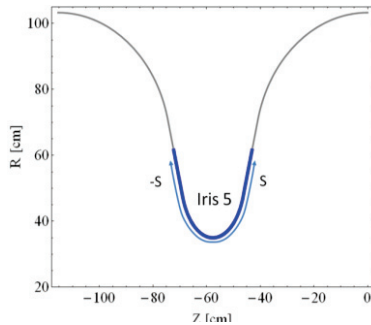


Fig. 4: Blue region is the field emitter region. Local coordinate was used as a function of distance (S) from the cavity iris along the cavity wall.

From simulation result, iris5 was divided into 6 parts and 3 kinds of typical long range trajectory (see Fig. 5) are found (see Fig. 6).

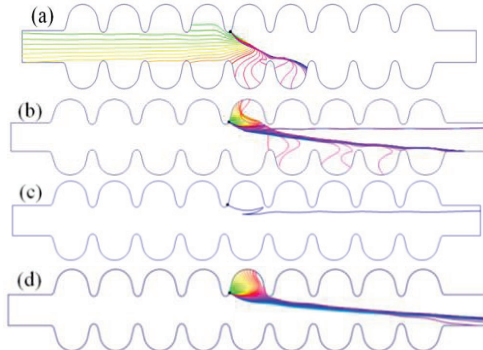


Fig. 5: Three kinds of typical long range trajectory; (a) trajectories from reverse region, (b) trajectories from zigzag region, (c) long range zigzag trajectory, (d) trajectories from forward region.

(1) Reverse regions, long range emission electrons from these regions can travel reversely and bombard at the opposite blank flange.

(2) Zigzag regions, some special long range emission electrons travel forward then backward and finally forward and hitting on the facing blank flange. Their trajectories look like a ‘Z’.

05 Cavity performance limiting mechanisms

R. Field emission & multipacting

(3) Forward type trajectory, long range emission electrons from these regions can travel forward and hit on the facing blank flange.

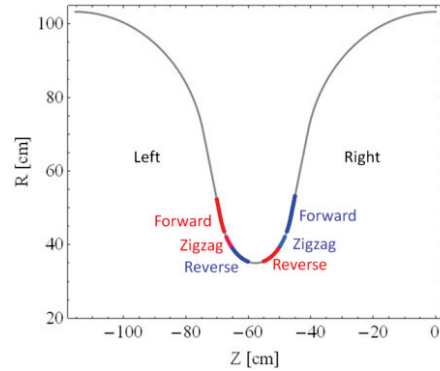


Fig. 6: Iris 5 was divided into 6 parts and 3 kinds of emission electrons with long range trajectory are found.

Long range electrons from IR_5_LF forward & zigzag region and IR_5_RT reverse regions (blue regions in Fig. 6) can hit left blank flange. Similarly, electrons from IR_5_RT forward & zigzag region and IR_5_LF reverse regions (red regions in Fig. 6) can hit right blank flange. These kinds of electrons can form dark current escaping from the cavity and accelerated in another cavity.

The impact energy of the emitted electrons from IR_5 is shown in Fig. 7. To simplify the discussion, we focus our attention on IR_5_RT. The initial phase of the emitter from IR_5_RT is from 118.8° to 241.2° (see Fig. 8). We can see that the long range of forward type emission electrons are launched from 118.8° (the beginning of emission) to 135° . Long range zigzag type emission electrons are near 145° and 180° and long range reverse type emission electrons are from 180° to 225° . In the simulation, the emission electrons are launched at radiofrequency phase interval $\Delta\phi = 0.48^\circ$.

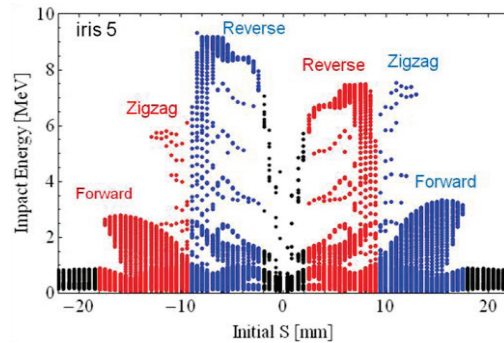


Fig. 7: Impact energy from 6 regions of iris 5 at gradient of 15MV/m.

Long range emission electrons will gain high energy from electromagnetic field. If they escape from a cavity and gain energy in the next cavities, they will become high energy dark current. They can cause activation and damage of accelerator components. Higher order modes can be excited by dark current in the cavity [10], which will lead to beam instability even beam break up.

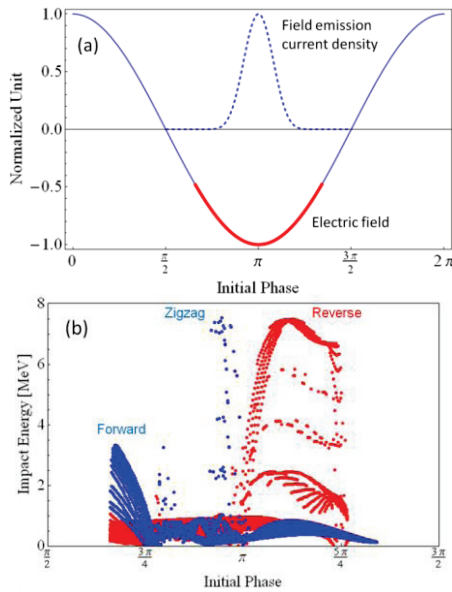


Fig. 8: Emitter phase with impact energy; (a) initial phase (red) with FE current density (dotted), (b) 3 long range trajectories are launch at different phase.

The emission electrons escaping ratio is defined as the emitted electrons escaping the cavity over the total emitted electrons considering the Fowler-Nordheim law. The hitting ratio is defined as the emitted electrons hitting on each cell or beam pipe. The escaping and hitting ratio of the emitter from right IR_5_RT at field gradient 15MV/m is shown in Fig. 9. We can see that reverse type emission electrons escaping ratio from left flange is high (blue line), especially at S=7.5mm about 55%. The zigzag and forward type emission electrons escaping from the cavity is about 6.5% at peak. Most of emission electrons will hit on the wall of cell5 (black line) except at the peak of reverse region. Fairly large amount of emission electrons will hit on the neighbor cells (cell4 and cell6). We will focus our attention on the emission electrons which will escape from the cavity.

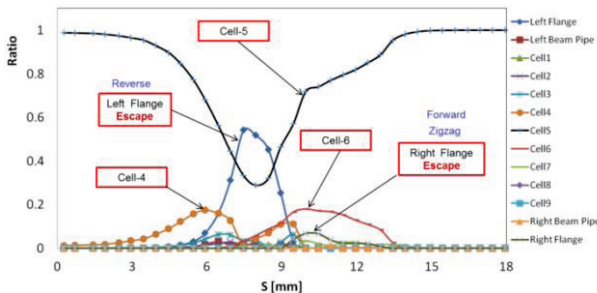


Fig. 9: Passing ratio of field emission electrons from right region of iris 5.

EXPERIMENT

ILC R&D cavity TB9RI-023 (RI23) is a field emission limited cavity. This cavity was used to benchmark our simulation model. The energy of long range emission electron will provide usefully information about the field emission in the cavity. For vertical test in dewar, it is not easy to measure the energy of the emission electrons

escaping from the cavity. However, the maximum of the energy of emission electrons can be determined by the end point energy of the Bremsstrahlung spectrum produced by electrons stopping in material [11]. So, we set up our system to measure the photon spectrum generated by the emission electrons (see Fig. 10). The Bremsstrahlung spectrum is measured at different fundamental modes. End point energies are obtained by exponential fit the Bremsstrahlung spectrum (see Fig. 11). Table 1 and Table 2 show the end point energies at different field gradient for π and $7/9 \pi$ mode separately. Field emission onset end cell gradient at other modes is shown in Table 3.

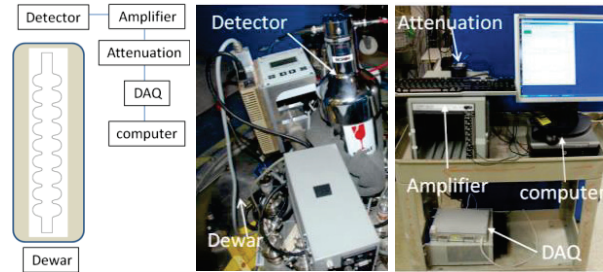


Fig. 10: left: Detector system Diagram, middle: NaI(Tl) scintillation, MODEL 4MT4/5L, BICRON CORP. right: DAQ system.

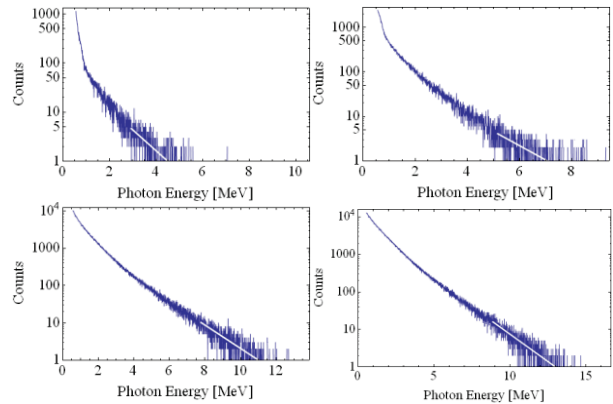


Fig. 11: Bremsstrahlung spectrum measured with NaI(Tl) scintillation (4.25 in. diameter, 4.5 in. length) for π mode accelerating gradient of 10 MV/m, 11 MV/m, 13 MV/m and 14 MV/m. The end point energies obtained by the exponential fit the Bremsstrahlung spectrum with an experimental accuracy of about $\pm 15\%$.

Table1: π Mode End Point Energy Fit

Gradient	End point Energy	Note
10MV/m	4.5MeV	FE starts @ about 9MV/m
11MV/m	7MeV	
12.1MV/m	9.1MeV	
13MV/m	11MeV	
14MV/m	13MeV	
15MV/m	15.1MeV	detector saturated
15.9MV/m	17.9MeV	detector saturated
17MV/m	13MeV	detector saturated

Copyright © 2013 by the respective authors

Table 2: 7/9 π Mode End Point Energy Fit

Gradient	End point Energy	Note
14MV/m	2.3MeV	FE starts at about 13.5MV/m
16.2MV/m	3.2MeV	
18MV/m	3.9MeV	
21MV/m	5.8MeV	
22MV/m	6.8MeV	
24MV/m	8.9MeV	
26MV/m	12.1MeV	detector saturated

Table 3: Field Emission at Other Modes

Mode	field emission onset (end cell gradient)
1/9 Pi	5.7 MV/m
5/9 Pi	28 MV/m
6/9 Pi	30 MV/m

For π mode, field emission starts at about 9MV/m. But for 6/9 pi mode, field emission onset is at 30 MV/m (end cell gradient). Considering the field distribution of 6/9 π mode (see Fig. 12), the dominant field emitter should be in cell1, 2, 5 or 8. For 1/9 π mode (see Fig. 12), field emission onset is 5.7 MV/m (end cell gradient) which is 32 MV/m for cell 5. So, the dominant field emitter is not in cell5. The focus is in cell 2 or cell 8 and they almost symmetrical for the 9cell cavity.

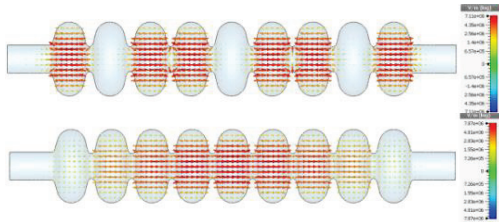


Fig. 12: Above: 6/9 Pi mode electric field distribution in 9cell cavity. The field strength is equal in cell 1, 3, 4, 6, 7 and 9. Electric field strength in Cell 2, 5, 8 are very weak compared with other cells. Bottom: 1/9 Pi mode electric field distribution.

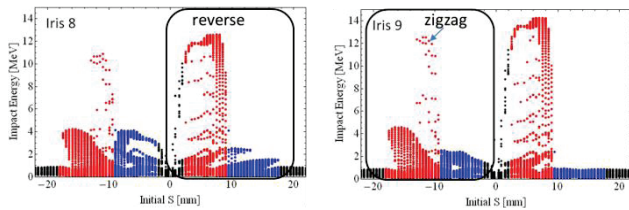


Fig. 13: Impact energy at iris 8 and iris 9.

Cell 8 is chosen to analyze the dominant emitter location. The field emitter is focus on IR_8_RT and IR_9_LF in cell 8. Considering the gradient with impact energy of Pi mode (See Table 1 and Fig. 13), the potential position is limited at IR_8_RT reverse region or IR_9_LF Zigzag region.

05 Cavity performance limiting mechanisms

R. Field emission & multipacting

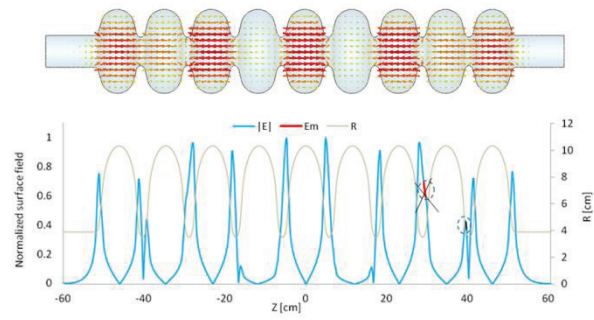


Fig. 14: 5/9 Pi model, electric field distribution and surface field distribution.

For 5/9 Pi mode, field emission starts at 28 MV/m (end cell gradient). Consider the 5/9 Pi mode surface field distribution (see Fig. 14), the IR_8_RT reverse region electric field is about 36 MV/m when the end cell gradient is 28 MV/m. For pi mode, the field emission is about 9 MV/m, which means the field emitter max surface electric onset is less than 18 MV/m. So, IR_8_RT reverse region is not the field emitter candidate and IR_9_LF Zigzag region is the only candidate in cell 8. Considering the symmetry of the cavity, the potential emitter location is at IR2-Zigzag or IL9-Zigzag region.

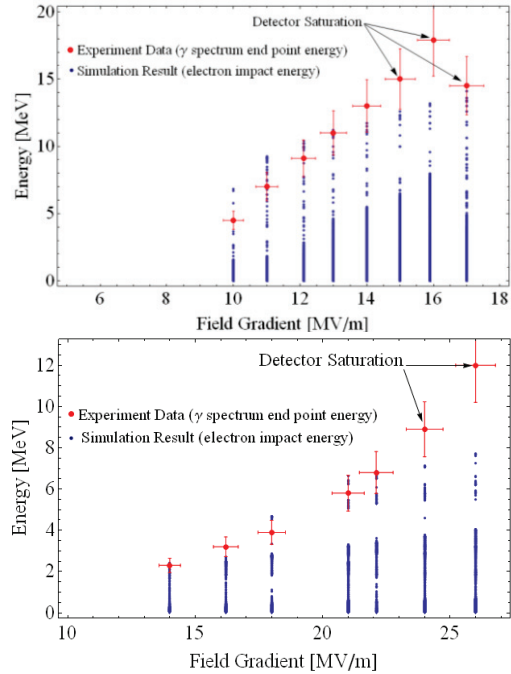


Fig. 15: Above: Photon spectrum end point energy and simulation electron impact energy at Pi mod. Bottom: Photon spectrum end point energy and simulation electron impact energy at 7/9 Pi mod.

Fig. 15 shows the impact energy of electrons from above region with end point energy of photon for π mode and 7/9 π mode. The photon spectrum end point energy agree very well with simulation electron highest impact energy for both π and 7/9 π mode. In our experiment, detector is not shielded. The radiation flux is so high at high field gradient that the detector is saturated. The detector can't separate two events and treat them as one

signal. Also, the gain of the photomultiplier tube based at high radiation will increase a little bit [12, 13]. Considering the two factors, the experiment data is higher when the detector is oversaturation at high accelerating field (high radiation flux).

RADIATION MEASUREMENT

In order to identify the emitter position, we put several Hamamatsu S1223-01[14, 15] silicon detectors around left flange and right flange. The data shows that the radiation voltage around left flange is 10 times higher than right flange. For zigzag region, most of the long range emission electrons will hit on the facing blank flange (see Fig. 5), which will generate lots of photon and the detectors around left flange had high radiation value. So, the field emission position is located at IR_9_LF zigzag region in cell 8. Fig. 16 shows the trajectories of the potential emission electrons from IR_9_LF zigzag region. More analysis of the radiation cause by emission electrons will talk at the follow paragraph.

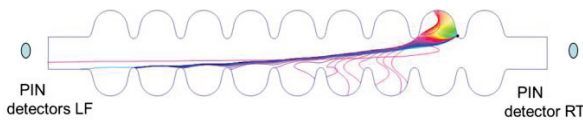


Fig. 16: Potential trajectory of the field emission electrons in the cavity. Diodes are placed at left and right flange.

From the photon energy measurement, the emitter is located at IR_9 Zigzag region and the potential range is from 9.4~12.9mm (S). But the rotation distribution of field emitter can't be approached by the photon energy measurement. In order to get the angular distribution, we put 6 diode rings on the iris of the cavity (see Fig. 17). Sixteen diodes are evenly distributed in each ring holder (see Fig. 18). The cavity was test at Pi mode at 2k and the diode ring signal are shown in Fig. 19. For different gradient the ring signal curve trend are almost the same and signal value goes up with gradient. A very distinguish signal was found at ring 1, where emitter was located at this iris. Ring 3 and 4 has asymmetry angular distribution which is 180 degree shift to the angular distribution of ring 1.

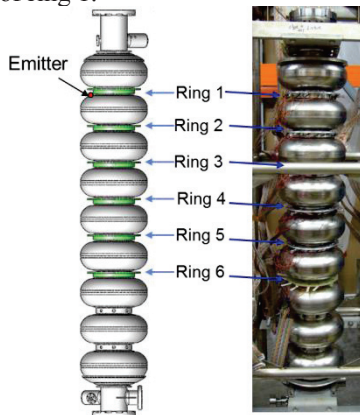


Fig. 17: Six diodes rings are mounted on the cavity. Left is the diagram of rings on the cavity and right is the picture of the six rings on the real cavity.

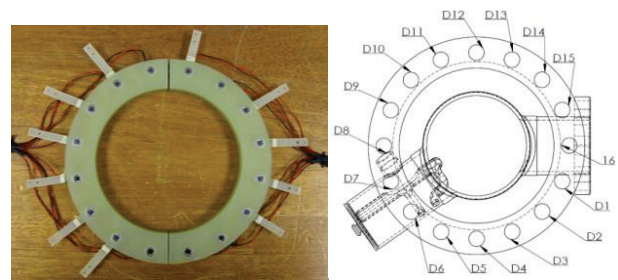


Fig. 18: Left: sixteen diodes are evenly distributed on the holder. Right: Diode ring angular distribution on the cavity view from beam pipe to cavity direction.

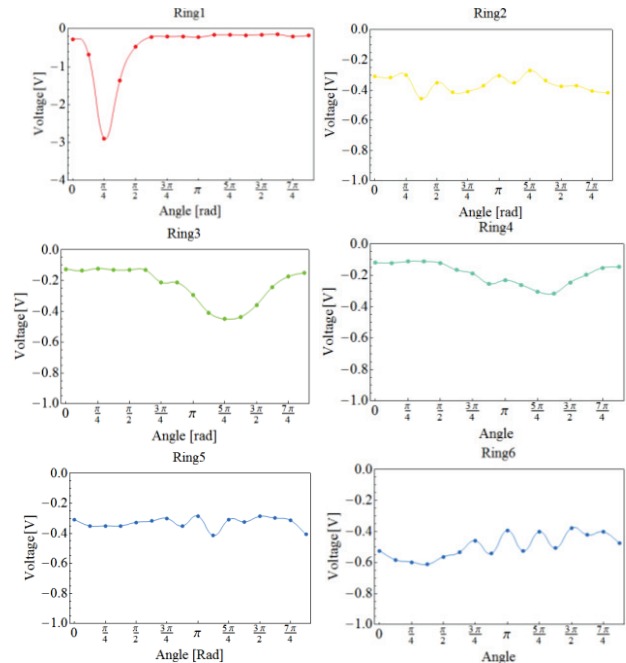


Fig. 19: Six diode rings signals @ 2k cold measurement.

SIMULATION OF PHOTON DISTRIBUTION

In order to find the connection between the field emission electrons and the diode rings signal. The impact electron information has been investigated. From the above analysis, the emitter is located within iris 9 (-12.9 to -9.4 mm, S coordinate) and the exact location can't located. The following analysis is the field emitter chosen at IR_9_RT -9.52mm (S). From the simulation, we can find that 78.8% of electrons are hitting on cell 8 and their energy is below 1 MeV (see Fig. 20). The electrons hitting on left flange or beam pipe is about 4% but their energy is around 13 MeV (at gradient of 17 MV/m). Simulation of the photon distribution is done by the program of Geant 4.9.4 [16] developed by CERN. The Low energy Electromagnetic Physics model [17] is used in our simulation. The impact electron energy information (energy, position, direction and quantity) are acquired from Track 3P. In the simulation, the detector is a continuous detector and totally covered the 9 cell cavity (See Fig. 21).

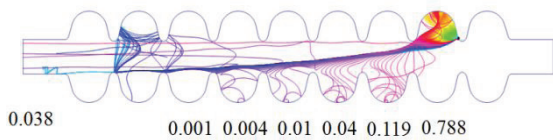


Fig. 20: Potential emission electrons hitting on the cavity wall. The number below the cavity represents the ratio of electrons hitting on each cell or flange.

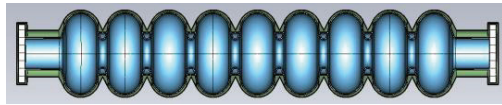


Fig. 21: The photon distribution was measured by a detector which is totally covered the cavity.

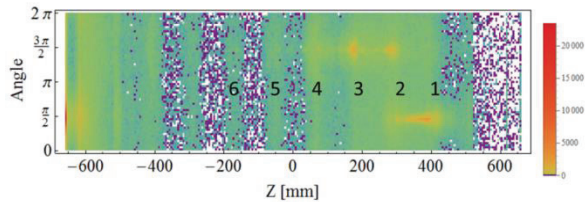


Fig. 22: Photon density distribution from Geant4 simulation. The number shown on the figure corresponds to the diode ring position. The right legend is the photon number in one RF period.

Photon density distribution is shown in Fig. 22. The x axis is defined as zero degree, so y axis is 90 degree. The emitter angle is 90° or $\pi/2$. From Fig. 22, the photon density at emitter place is high compare with other iris place. At ring 3 and 4 location, high photon density area is also found, which is 180° shift to the emitter location. Ring 2 seems to have two peak photon density area with 180 degree shift. The photon density at left flange is much high than the left flange. The photon density distribution agrees well with our experiment data distribution.

The simulation of the photon response in diode will be done in the next step.

OPTICAL INSPECTION

After cryogenic RF testing, the cavity was opened and optical inspected by Kyoto camera [18] (resolution of about $7.5 \mu\text{m}/\text{pixel}$). No distinguish defect was found at the predicted field emitter location and other iris area. It gives hints that the field emitter is less than the camera resolution.

SUMMARY

Systematic analysis of the behaviours of field emitted electrons is obtained using the ACE3P code developed by SLAC. Experimental benchmark of the procedure was carried out in cryogenic testing of a 9-cell cavity. From the field emission onset surface field and end point energy of photon spectrum, the location place was located to two zigzag regions. With the information of diodes placed around both the flanges, the emitter was located to one zigzag region. Angular location of the field emitter is determined by placing an array of silicon diodes around

irises of the cavity. Simulation of the photon distribution generated by emission electrons was done by Geant 4. The preliminary result agrees well with the experiment data. After cryogenic RF testing, the cavity was optical inspection with Kyoto camera, no outstanding feature was found at the predicted location and other iris, suggesting the size of the field emitter is below the detection limit of the optical inspection system. Future work will extend the developed procedure for generic use of field emitter localization in full scale cavities during vertical test or in cryomodule testing.

REFERENCES

- [1] B. Aune, R. Bandelmann, et al, Superconducting TESLA cavities, PRST-AB, VOL 3, 092001 (2000).
- [2] K. Welch et al., Accelerator Safety Workshop, http://www.aps.anl.gov/News/Conferences/2011/ASWorkshop/files/12_Kelsey.pdf (2011).
- [3] C. E. Reece et al., Proc. of PAC 2005, 0-7803-8859-3 4081 (2005).
- [4] K. Ko et al, Advances in Parallel Electromagnetic Codes for Accelerator Science and Development, LINAC2010, Tsukuba, Japan.
- [5] Cho-Kuen Ng, Nathan Folwell, et al, Simulating dark current in NLC structures, Nuclear Instruments and Methods in Physics Research A 558 (2006) 192-195.
- [6] Padamsee H, Knobloch J, Hays T. RF Superconductivity for Accelerators. New York: John Wiley & Sons, Inc., 1998. 232-234.
- [7] H.A Schwettman, J.P. Turneure and R. F. Waites, Evidence for surface-state-enhanced field emission in rf superconducting cavities, J. Appl. Phys. 45, 914, 1974.
- [8] C. Lyneis, Y. Kojima, et al, Electron loading in L and S band superconducting niobium cavities, IEEE, 20, 101 – 103, 1973.
- [9] S. Musser, J. Bierwagen, et al, X-ray imaging of superconducting rf cavities, Proceedings of the 12th International Workshop on RF Superconductivity, TUP27.
- [10] V. Volkov, Monopole passband excitation by field emitters in 9-cell TESLA-type cavities, PHYSICAL REVIEW SPECIAL TOPICS - ACCELERATORS AND BEAMS 13, 084201 (2010).
- [11] R.P Lambert, J.W. Jury and N.K. Sherman, Nuclear Instruments and Methods 214 (1983) 349-360.
- [12] S.Bianco, F.L Fabbri, et al, A study of the short-term rate in Philips XP-2008 photomultiplier tubes, Nucl. Instr. And Meth. A301(1991) 279-287.
- [13] Cao Zhong, Huang Zhengde and Chen Qun, GAIN STABILITY OF PHOTOMULTIPLIERS AT HIGH VARIABLE COUNTING RATES, Nucl. Instr. And Meth. A281 (1989) 384-387.
- [14] <http://sales.hamamatsu.com/en/products/solid-state-division/siphotodiode-series/si-pin-photodiode.php>, April23 (2012).
- [15] A. D. Palczewski and R. L. Geng, Proceedings of IPAC2012, New Orleans, Louisiana, USA, WEPPC095.
- [16] <http://geant4.cern.ch/>
- [17] <https://twiki.cern.ch/twiki/bin/view/Geant4/LowEnergyElectromagneticPhysicsWorkingGroup>
- [18] Yoshihisa Iwashita and Yujiro Tajima, PHYSICAL REVIEW SPECIAL TOPICS - ACCELERATORS AND BEAMS, 11, 093501 (2008).